

Article

Improving Lidar Windshear Detection Efficiency by Removal of “Gentle Ramps”

Kai Kwong Hon *  and Pak Wai Chan

Forecast and Warning Services, Hong Kong Observatory, Kowloon, Hong Kong; pwchan@hko.gov.hk

* Correspondence: kkhon@hko.gov.hk

Abstract: The Doppler Lidar windshear alerting system at the Hong Kong International Airport (HKIA), the first of its kind in the world, has been in operation since 2006. This paper reports on an enhancement to the automatic windshear detection algorithm at HKIA, which aims at filtering out alerts associated with smoother headwind changes spread over longer distances along the aircraft glide path (called “gentle ramps”) which may nonetheless exceed the well-established alerting threshold. Real-time statistics are examined over a 46-month study period between March 2016 and December 2019, covering a total of 2,017,440 min and over 1500 quality-controlled pilot reports of windshear (PIREP). The “gentle ramp removal” (GRR) function is able to effectively cut down the alert duration over the 5 major runway corridors, inclusive of both landing and take-off, which together account for over 98% of the PIREP received at HKIA during the study period. In all 5 runway corridors this is achieved with a proportionately smaller decrease—even with no changes in 2 cases—in the hit rate, highlighting the efficiency of the GRR function. The difference in statistical behaviour across the runway corridors also echo literature findings about the differences in length scale of wind disturbances at different locations within HKIA. This study serves as a unique documentation of the state-of-the-art in operational Lidar windshear detection and can provide useful reference to airports and aviation meteorologists around the world.

Keywords: Lidar; wind shear; turbulence; airport; Hong Kong; boundary layer; verification



Citation: Hon, K.K.; Chan, P.W. Improving Lidar Windshear Detection Efficiency by Removal of “Gentle Ramps”. *Atmosphere* **2021**, *12*, 1539. <https://doi.org/10.3390/atmos12111539>

Academic Editor:
Alexandros Papayannis

Received: 10 September 2021
Accepted: 18 November 2021
Published: 22 November 2021

Publisher’s Note: MDPI stays neutral with regard to jurisdictional claims in published maps and institutional affiliations.



Copyright: © 2021 by the authors. Licensee MDPI, Basel, Switzerland. This article is an open access article distributed under the terms and conditions of the Creative Commons Attribution (CC BY) license (<https://creativecommons.org/licenses/by/4.0/>).

1. Introduction

Low-level windshear, operationally defined as sustained headwind changes at an altitude of 500 m (interchangeably with 1600 feet) along the aircraft flight path [1,2], is a recognised aviation safety hazard. The consideration of the headwind, or wind blowing in the opposite direction to the aircraft flight direction, is important for two reasons. Firstly, an aircraft in motion relies on headwind to provide buoyancy; a sudden change in headwind component alters the buoyancy and consequently the altitude of the flight trajectory. Secondly, during the landing or take-off phases of flight, the aircraft is in close proximity to the ground while having relatively low airspeed (e.g., as compared to the level phase of flight at cruising altitude). This leaves little room for manoeuvre using trade-offs between speed and altitude [3], in case of sudden, significant changes in buoyancy. For windshear under clear air conditions (i.e., not accompanied by precipitation), the Doppler light detection and ranging (Lidar) has gained recognition as an effectively solution in detection and automatic alerting [4]. The Lidar remotely senses the environmental wind field through detecting the Doppler effect on the backscattered laser beam from aerosols advected by the air motion in each scanning volume. The long-range Doppler Lidar, typically having a radial range of 8–10 km or above, is characterised by high radial resolution of about 100 m and fast revisit times on the order of minutes for full-disc planar scans (or plan-position indicator, PPI), and is used in various applications in the atmospheric sciences.

The Hong Kong International Airport (HKIA) is well-known for its susceptibility to low-level windshear [5,6]. HKIA is situated on an artificial island surrounded on

three sides by open waters and flanked to its south by the mountainous Lantau Island (Figure 1). The Lantau Island is orographically complex and has peaks up to 900 m tall which are interspersed by valleys about 300 to 400 m above sea level. Clear air (or “dry”) windshear may be caused by two main factors, the disruption of background wind flow by the Lantau terrain, and intrusion of sea breeze fronts. At HKIA, the Hong Kong Observatory (HKO) employs long-range Doppler Lidar for performing real-time automatic detection and alerting of low-level windshear since 2006. This is the first such system in the world. In addition to providing operational support to HKIA, the Lidars have supported various research studies on complex geophysical airflows including both observation and modelling aspects [7–9]. Over the past decade or so, different attempts have been documented with the aim of enhancing the efficiency of the Lidar windshear alerting algorithm at HKIA. These include combining different types of Lidar-based wind change detection principles to increase overall hit rate [10], using alternative metrics such as the eddy dissipation rate as the alerting threshold [11], and even switching to the spectral or Fourier space [12]. However, it is unfortunate that these experimental algorithms have not been able to enter into the sphere of real-time operation. The difficulties are two-fold. Firstly, aviation users at HKIA have expressed a preference for greater “economy” of alerts, meaning that they prefer fewer alerts to be issued overall, where safe and practicable. This means that addition of new detection principles, which necessarily broadens the set of alerts, is in general less favoured. Secondly, alerts are preferably issued based on physically intuitive and easy-to-understand quantities. This means that technically complex physical parameters, such as the eddy dissipation rate and power spectrum coefficients, are less suitable than simple thresholds based on the headwind.

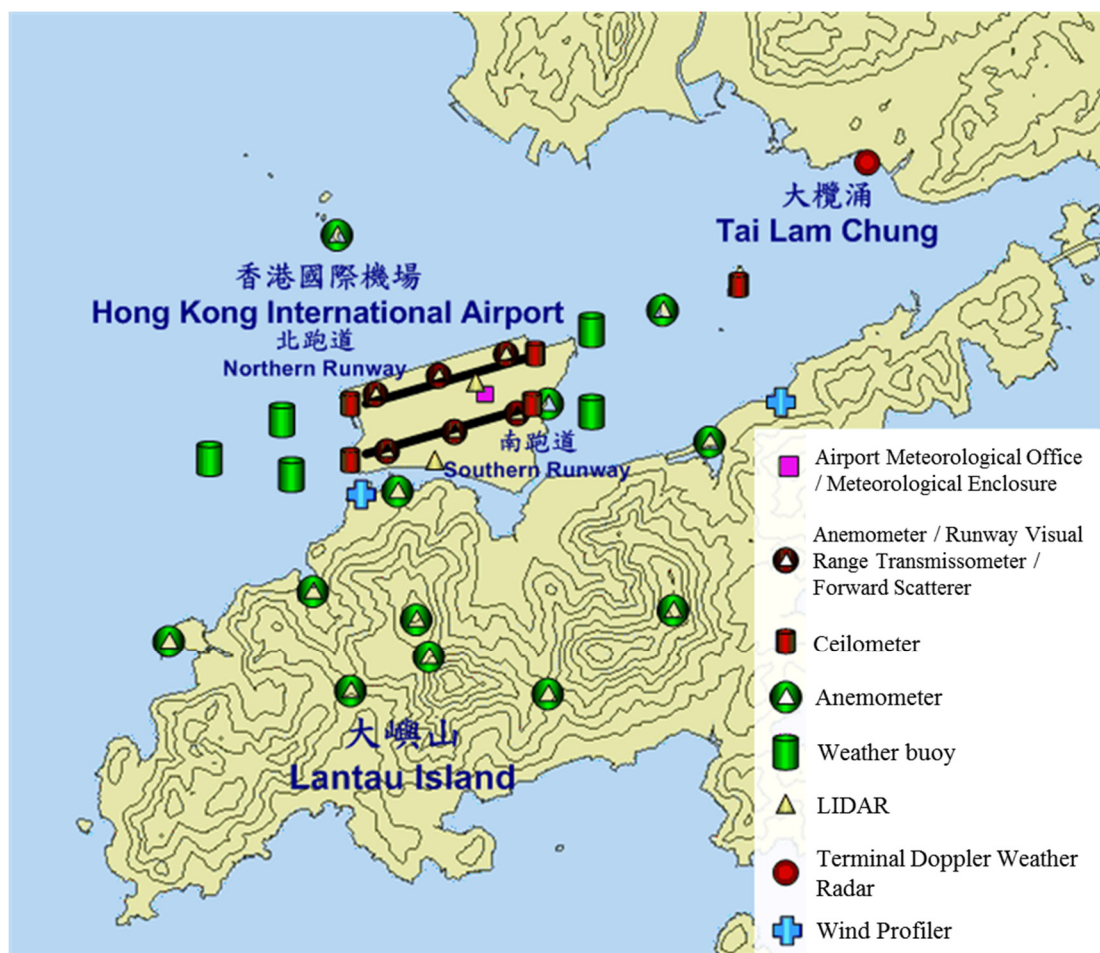


Figure 1. Schematic diagram of Hong Kong International Airport and location of Doppler Lidars.

The problem of windshear detection using Doppler Lidar has been studied at many major airports around the world. For example, at the Beijing Capital International Airport [13], Lidar with radial resolution of 30 m has been used to detect small scale wind disturbances suspected to be caused by nearby buildings and rows of trees. Furthermore, terrain-induced windshear is studied using optimised scanning strategy along the glide path during certain favourable wind regime [14]. At the Narita International Airport [15], Lidar observation data has revealed the role of horizontal convective rolls in inducing windshear. At Nice Côte d’Azur international airport [16], horizontal windshear is studied using Lidar, wind profiler and anemometers as well as numerical simulations. At the Bratislava Airport [17], Lidar has been employed to detect windshear occurrence due to a number of meteorological factors such as thermodynamic inversion, cold front and gust front. At Frankfurt and Munich International Airports [18], a system consisting of Lidar and X-band polarimetric scanning radar is used to detect gust front, microburst and vertical shear. The above studies highlight the fact that, while advanced remote-sensing instruments such as the Doppler Lidar are demonstrated to be effective in capturing the phenomena of low-level windshear, the underlying meteorological and geographical factors contributing to its occurrence may differ considerably across airports. Furthermore, the length of study periods in the above examples also differ, ranging from case studies to covering several months or seasons of a year. As such, it may not be possible to directly compare statistical behaviour or detection performance across different regions or airports, despite the safety implications and apparent universality of the underlying meteorological phenomenon.

In this study, we present the real-time performance of the “gentle ramp removal” (GRR) function, which is an enhancement to the Lidar windshear alerting algorithm operationally implemented at HKIA with aviation users’ support. The GRR function aims at cutting down the alert duration of Lidar-based windshear alert to better match the perception of aircraft pilots landing at and taking off from HKIA, who are the prime audience of the windshear alerts provided by HKO. This study is unique in a number of aspects. First, it is based on an operational alerting system which is in daily use at a major aviation hub, instead of post-analysis using field measurement data. Secondly, the study period, spanning close to 4 years in continuous real-time operation, is among the longest reported in the literature. Thirdly, the number of quality-controlled pilot reports involved, at over 1000, is also among the largest when compared to any reported study. Fourth, as will be discussed in Section 4, this may be the first study dealing specifically with objective means for “trimming down” or systematically reducing the issuance of Lidar windshear alerts. Finally, while most previous reports deal with one or two commonly used runway configurations at a time at the corresponding airport, in this study the proposed GRR function is successfully applied to all 8 runway configurations at HKIA. This paper is organised as follows. Section 2 provides a technical description of the long-range Doppler Lidars in use at HKIA, the operational low-level windshear alerting algorithm (GLYGA), and the pilot reports of windshear used for validation. The improvement to the GLYGA algorithm, namely the “gentle ramp removal” (GRR) function, is described in Section 3. Section 4 presents and discusses the results of the improved alerting algorithm including long-term validation. Section 5 concludes the paper.

2. Instrument and Data

In this section, the windshear detection instruments, namely the Doppler Lidar, and the associated data processing including the Lidar windshear alerting algorithm, as well as validation data set, namely pilot reports, will be described in detail.

2.1. Doppler Lidars at HKIA

In this study, output data from the two operational long-range Doppler Lidars at HKIA will be used. Location of the two Lidars are shown in Figure 1. The two long-range Doppler Lidars are manufactured by Mitsubishi. They operate at the infrared wavelength

of about 1.5 microns. The radial resolution, or physical range gate, is 100 m. The maximum unambiguous radial velocity is about 40 m/s. Under fine weather and unobstructed by weather phenomenon such as low clouds, typically an observation range up to 10 or 15 km is attainable. In addition to performing routine fixed-elevation scans (plan-position indicator or PPI), each Lidar is configured to provide dedicated “glide-path” scans along take-off and landing flight paths. This is achieved by a concerted motion of the elevation and azimuthal directions of the laser scanner head. Normally, the North Lidar covers the four possible configurations of the North Runway (known as 07LA, 25RA, 07LD and 25RD) and the South Lidar covers the four possible configurations of the South Runway (known as 07RA, 25LA, 07RD and 25LD), including both arrival (abbreviated as “A”) and departure (“D”) directions towards the west and the east. From the radial velocity data collected by the “glide-path” scans, the headwind component along each runway configuration (known as “corridor”) may be derived. These are output in the form of a headwind profile. Typically, the scan revisit time of each corridor is about 1 min, which means that the headwind profiles have temporal resolution or update frequency of about 1 min.

The study period covers March 2016 to December 2019 which is 3 years and 10 months in duration. The Lidars may be assumed to have full availability during the period, since operational arrangements are in place for each Lidar to serve as mutual back-up of the other in case of maintenance needs. Scanning range of the Lidars may also be impaired during foggy and rainy situations. In significant instances such as passage of typhoons or heavy rain, the usable range may fall below 500 m. However, these are relatively rare occurrences in practice, and other meteorological instruments (notably the Terminal Doppler Weather Radar) will readily work in rainy conditions to provide effective scanning and corresponding windshear alerts. For the purpose of this study, full availability will be assumed in the calculations below without the need to account for maintenance or downtime (i.e., taking the length of the study period to be 46 months, or equivalently 2,017,440 min).

2.2. Lidar Windshear Alerting Algorithm

The operational Lidar windshear alerting algorithm for HKIA is known as “GLYGA”. Technical details of GLYGA have been discussed at length in [4]. Here we describe the salient features of the algorithm (Figure 2). For each runway corridor, GLYGA takes as input the profile of headwind components gridded at fixed spacing of about 100 m. The headwind profiles typically extend up to about 4–5 NM from the corresponding runway endpoint, depending on scanning range and prevailing atmospheric conditions at the time. A ramp identification procedure is then applied to identify abrupt, sustained changes in the headwind. This is based on the concept of the “Peak Spotter” algorithm of [19]. First, a profile of velocity increment is computed by taking the difference between adjacent data points in the quality-controlled headwind profile. Next, windshear “ramps” are detected by successively identifying the velocity increment (i.e., headwind change) within increasing length windows of 400, 800, 1600, up to 6400 m. The collection of such “ramps” identified within a single headwind profile is then prioritised using a severity factor following [20] which scales with the headwind increment and the inverse cube root of the corresponding ramp length. Among those ramps with intensity (i.e., headwind increment) exceeding the predetermined operational threshold at HKIA (14 kt), the ramp with the highest severity factor will be used to issue an automatic alert.

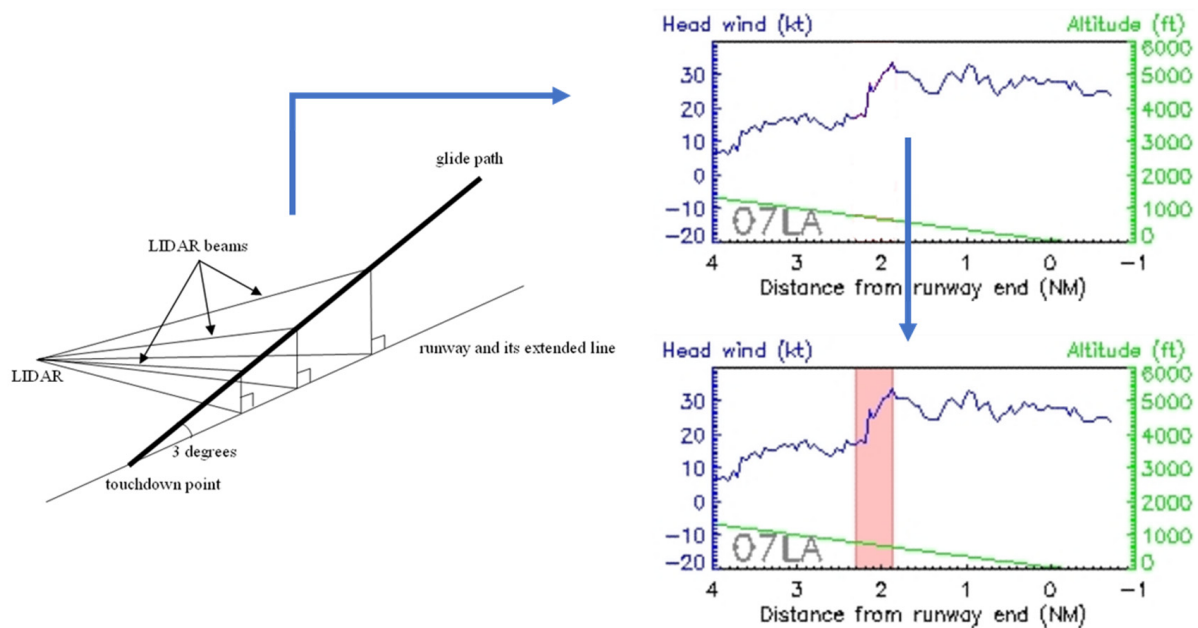


Figure 2. Schematic diagram of data processing in GLYGA algorithm.

Mathematically, we may denote the quality-controlled headwind profile as $v(x_i)$ where v is the headwind component at position x_i which is the i -th data point or range gate along the corresponding glide path. For a given length window (or ramp length) H , the velocity increment at position x_i can be expressed as $\Delta v(x_i, H) = v(x_i) - v(x_i + H)$. (Readers are referred to [4] for a detailed description of the ramp identification procedure in use at HKIA.) The resultant identified ramps, equivalent to a collection of data pairs $(\Delta v, H)$, are then prioritised with the severity factor S which is calculated following the formula:

$$S = \left(\frac{\Delta v}{H^{1/3}} \right)^3 / V_{app} \quad (1)$$

where V_{app} is the approach speed of the aircraft which may be taken as a constant. As mentioned above, this means that S depends primarily on $\Delta v/H^{1/3}$.

The above implementation of the GLYGA algorithm has been in use since the Lidar Windshear Alerting System (LIWAS) commenced operation at HKIA in 2006 [21]. Its real-time performance over the past decade have been routinely documented both internally for the aviation community as well as in various scientific studies covering different periods [22–24]. Typically, the performance of GLYGA can be characterised by a reasonable hit rate around 50–70% at a very low alert duration of around 2–4%, which might vary slightly year by year depending on the actual weather conditions. For the purpose of this paper, “GLYGA” will refer to the original implementation (i.e., before application of the “gentle ramp removal” function described in Section 3).

2.3. Pilot Reports (PIREP) of Low-Level Windshear

Pilot reports (PIREP) of low-level windshear is a well-established means for validating windshear alerts at HKIA. Typically, pilots of landing and departing aircraft may provide reports of low-level windshear (and turbulence, which is considered to be a separate phenomenon in terms of reporting and alerting at HKIA) encounters to air traffic control either directly through onboard radio communication or by submitting a report form afterward. We make a passing note that this is different from conventional PIREP of turbulence and icing, which normally cover the en-route phase of flight. The HKIA windshear PIREP contain information on the timing, location (normally reported to the nearest nautical mile), altitude (normally reported to the nearest 50 or 100 ft), and perceived

intensity (normally reported to the nearest 5 kt, e.g., –25 kt, with positive or negative signs representing gain or loss in head wind, respectively) of an event. All received PIREP underwent quality control by trained meteorological personnel to flag out those reported events that fall outside the scope of HKO’s low-level windshear alerting service, namely that the reported absolute magnitude must be 15 kt or greater, and that the location of occurrence must be below 1600 ft (used interchangeably with 500 m) or within 3 NM from touchdown/take-off.

The distribution of quality-controlled PIREP received during the study period is shown in Figure 3. Over the 46-month period, there are a total of 1557 valid events of low-level windshear at HKIA. As seen from the histogram, these are not evenly distributed, but concentrated over a smaller number of corridors. For example, 07LA contains the largest portion at 47.8% (745 events). Next is 25RA with 25.2% (393 events). 07RD, 07RA and 25LD, respectively, carries 10.4%, 8.5% and 6.2% (162, 132 and 96 events). There were 27 events over 25LA (1.7%) and only 1 event each over 07LD and 25RD (both 0.06%). Considering the relative numbers of event occurrence, in the subsequent sections we will focus on the statistics for 5 corridors: 07LA, 25RA, 07RD, 07RA and 25LD.

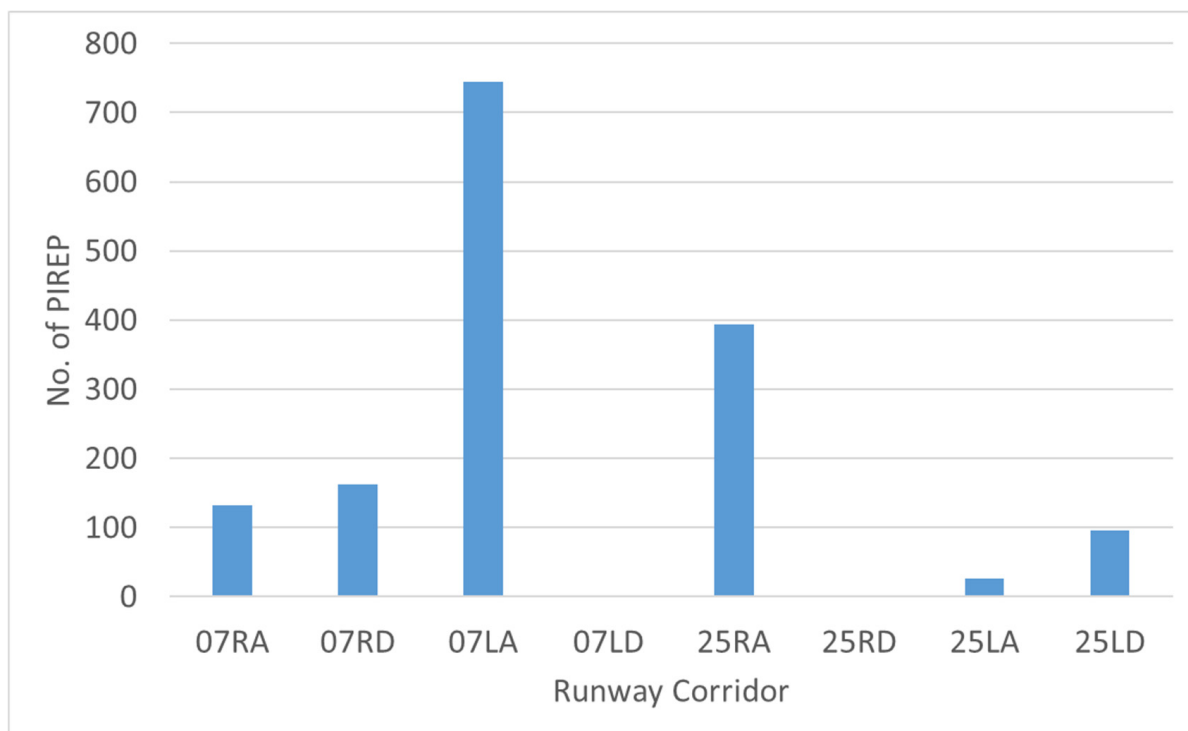


Figure 3. Distribution of windshear PIREP across the HKIA runway corridors during the study period.

3. Removal of “Gentle Ramps”

This section describes the background and the methodology of “gentle ramp removal” (GRR). After nearly a decade of real-time operation of the Lidar windshear alerting system and the GLYGA algorithm, HKO had received various feedback and comments from users of the aviation community regarding the phenomenon of windshear as perceived onboard in the cockpit as well as the provision of windshear alerts to aircraft. One aspect relates to the issuance of alerts for situations where a headwind change occurs in a smooth, gradual manner over a relatively long distance along the flight path which nonetheless exceeds the adopted alerting threshold of 14 kt. Such relatively gentle headwind changes are considered by pilots to pose relatively low impact to the control of the aircraft and hence aviation safety and may therefore be safely removed from the operational alerting system.

In consultation with aviation users, a scheme was developed for quantifying and identifying these gentle windshear ramp events, or simply “gentle ramps”. First, a typical

length scale is required to determine whether a particular windshear ramp identified by GLYGA might fall with the domain of “gentle ramps”. This length scale is set at 3 km or 3000 m. A physical interpretation of this value can be given as follows. For a commercial aircraft near touchdown, its typical ground speed would be roughly 150 kt or 77 m s^{-1} . A distance of 3000 m would translate to aircraft flight time of about 39 s, which might be considered a relatively long period of time (or equivalently distance) if the corresponding GLYGA alert is only triggered by a single sustained headwind change. Next, for those headwind profiles with the GLYGA-generated windshear ramp exceeding 3000 m in length, the degree of headwind fluctuations is measured. This is achieved by computing the root-mean-square (RMS) difference of the original headwind profile from its running mean. If this RMS measure of fluctuations falls below a certain threshold, the corresponding automatic windshear alert (as originally generated by GLYGA) would be withheld. This threshold is set at 1.2 kt with endorsement by aviation users. In summary, the GRR procedure may be encapsulated in the following steps:

(We highlight in bold text the new steps introduced.)

- (1) Given a particular Lidar headwind profile $v(x_i)$, the original GLYGA algorithm identifies the windshear ramp, characterised by $(\Delta v_0, H_0)$, possessing the maximum severity factor S .
- (2) **Check the intensity of the windshear ramp:**
 - (3.2) If $\Delta v_0 < 14 \text{ kt}$, no windshear alert will be issued (same as original design).
 - (3.3) **If $\Delta v_0 \geq 14 \text{ kt}$, perform additional check.**
- (3) **Check the length of the windshear ramp:**
 - (3.1) If $H_0 \leq 3000 \text{ m}$, the windshear alert will be issued (same as original design).
 - (3.2) **If $H_0 > 3000 \text{ m}$, perform additional check.**
- (4) **Check the RMS fluctuation:**
 - (4.1) **Compute the RMS fluctuation:**

$$\Delta v_{RMS} = \sqrt{\frac{1}{N} \sum_{i=1}^N [v(x_i) - \tilde{v}(x_i)]^2} \quad (2)$$

where N is the number of data points in the quality-controlled headwind profile and $\tilde{v}(x_i)$ is the mean headwind profile obtained by applying the running mean.

- (4.2) **If $\Delta v_{RMS} \geq 1.2 \text{ kt}$, the windshear alert will be issued (same as original design).**
- (4.3) **If $\Delta v_{RMS} < 1.2 \text{ kt}$, the windshear alert will be withheld.**

An example of the application of the GRR procedure is given in Figure 4. This is taken from a case on 20 November 2012 when the operational GLYGA issued a windshear alert over corridor 07LA but HKO subsequently received feedback that the associated wind change was not considered to be significant windshear by the pilot. The top panel of Figure 4 shows the Lidar headwind profile corresponding to the minute when the aircraft landed over 07LA. The region highlighted in blue shows the headwind ramp identified and alerted by GLYGA in real-time. The bottom panel of Figure 4 shows an analysis based on the GRR procedures. It could be seen that in the original headwind profile, a sustained change of headwind from 2 kt to 19 kt (i.e., magnitude of 17 kt) indeed occurred between the 4 NM and 2 NM marks. The length of this ramp as identified by GLYGA is 1.8 NM which is equivalent to 3.3 km. After computing and subtracting the mean headwind profile, it could be seen that the degree of headwind fluctuations is relatively small, within 2 kt at nearly all the positions along the glide-path. Here the RMS fluctuations is calculated to be 0.73 kt which is well below the chosen threshold of 1.2 kt. As such, this alert originally issued by GLYGA would have been effectively removed by GRR in agreement with the pilot’s perception at the time.

The GRR procedure has been implemented in real-time on top of the GLYGA algorithm since the beginning of 2016 (i.e., covering the start of the study period). To track

its operational implementation and effectiveness of performance, data will be recorded whenever GRR is triggered. This allows long-term monitoring and validation of the GRR procedure. The resulting data is analysed and discussed in Section 4.

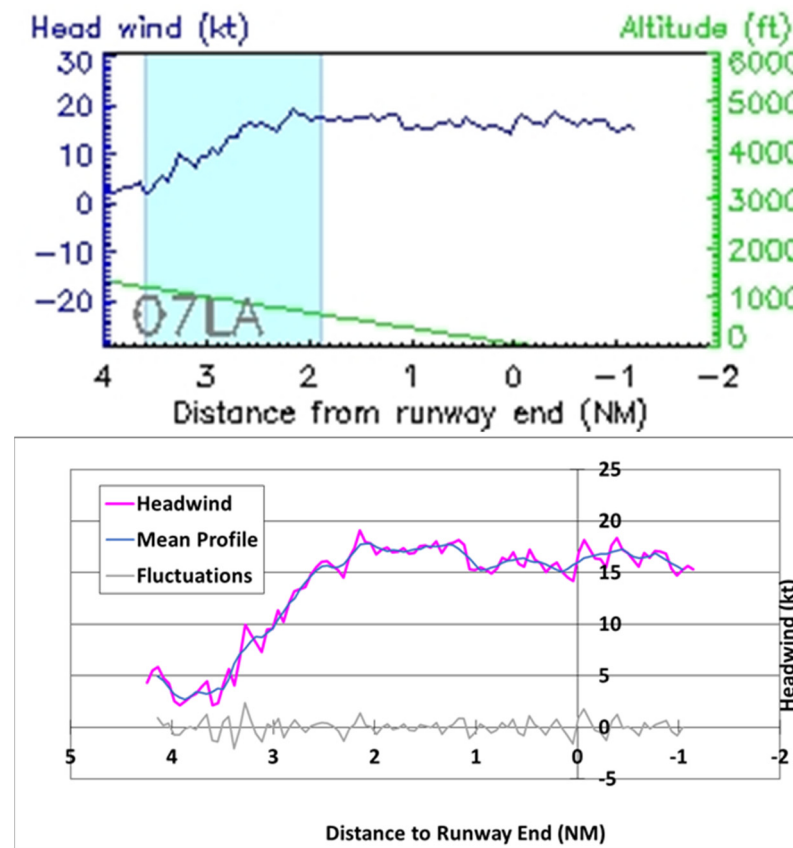


Figure 4. Headwind profile and windshear alert (highlighted in blue) issued by GLYGA for a case in 20 November 2012 (**top**). Analysis using the GRR procedures is shown in the (**bottom**).

4. Results and Discussions

In this section, we present and discuss the statistics of the real-time application of GRR. As mentioned in Section 2, the study period covers 46 months from March 2016 to December 2019, a total of 2,017,440 min. Out of the 8 possible runway configurations, the 5 corridors with the highest numbers of windshear reports received are studied, namely 07LA, 25RA, 07RD, 07RA and 25LD. To evaluate the effectiveness of GRR in removing potential windshear alerts, we inspect the Alert Duration which is the percentage of time during which a windshear alert is issued and in force. GLYGA alerts are updated every minute and therefore the Alert Duration may be calculated as the number of alerts issued for that runway corridor divided by the total number of minutes within a particular time period, namely:

$$\text{Alert Duration} = \frac{\text{No. of GLYGA alerts issued for that corridor}}{\text{Length of study period in minutes}} \quad (3)$$

The monthly time series for 07LA is shown in Figure 5a. The graph shows the monthly variation in Alert Duration before and after the application of GRR. Here the grey histograms are the Alert Duration after application of GRR. The blue segments represent the reduction in Alert Duration compared to the original GLYGA algorithm. It can immediately be seen that, while the extent may vary month-by-month, the GRR procedure is able to effectively reduce the Alert Duration in a general manner. Here the monthly or seasonal variation may be attributed to the weather conditions affecting HKIA

such that in certain months (mainly spring and summer) the atmospheric environment becomes more conducive to the occurrence of windshear. For months with relatively high Alert Duration, such as April 2014, March 2017, February to April 2019, the reduction in monthly Alert Duration ranges between 2.9% to 5.7%. In some instances, the Alert Duration may be cut down by half or more, such as February 2017 (3.8% to 1.3%), March 2017 (8.1% to 2.7%) and February 2019 (9.4% to 3.7%). For other months with relatively low Alert Duration originally (such as those with original Alert Duration below 1%), there are still small reductions which may range between 0.02% (October 2019) and 0.54% (December 2016).

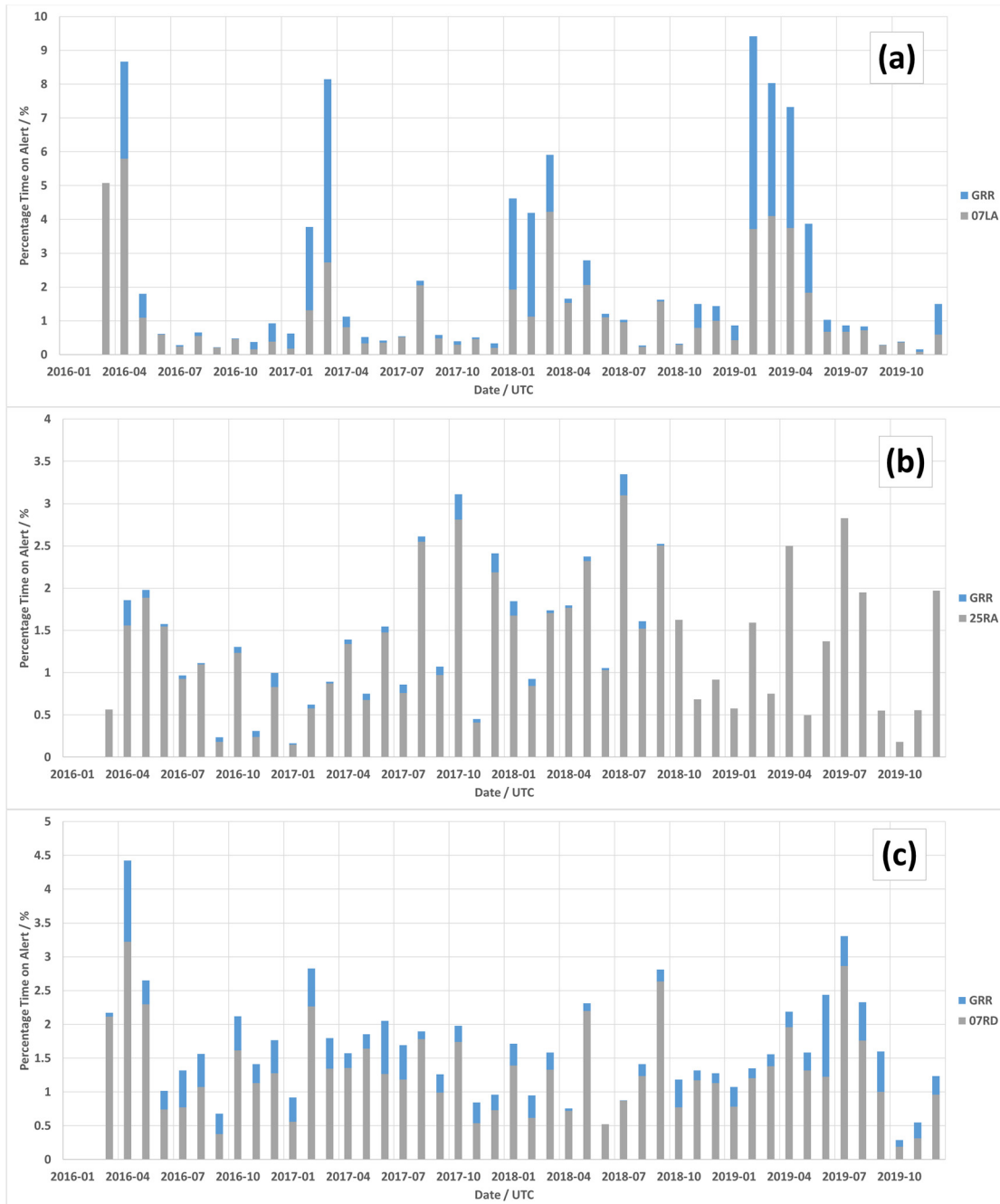


Figure 5. Cont.

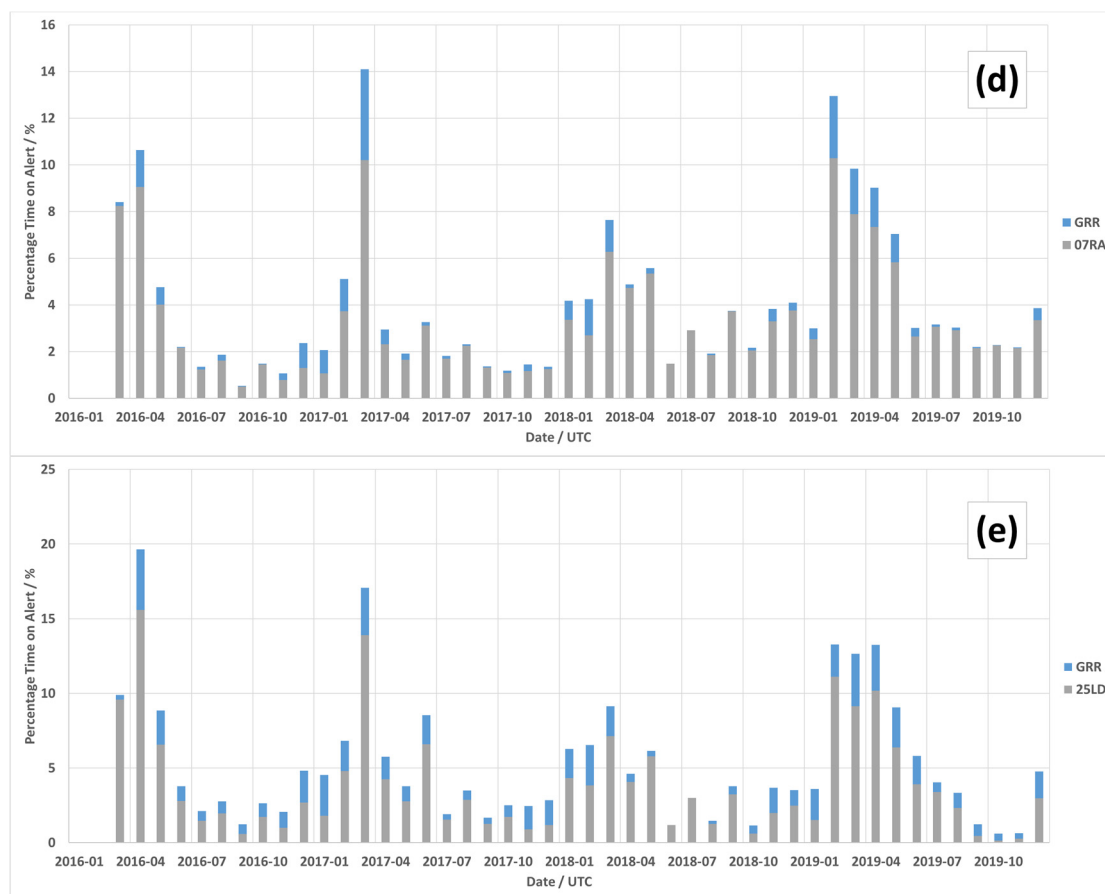


Figure 5. Effect of GRR on GLYGA alert duration over the 5 main runway corridors: (a) 07LA, (b) 25RA, (c) 07RD, (d) 07RA, (e) 25LD.

Statistics for the other runway corridors, namely 25RA, 07RD, 07RA and 25LD, are shown in Figure 5b–e. It could be seen that the monthly or seasonal variation behaviour differs across corridors. This is because the runway usage and hence direction of flight at the time of take-off or landing, depends on the prevailing wind direction at that instant. Corridors 07LA and 07RA both land from east to west, respectively, using the North and South Runway. As such, they share rather similar monthly and seasonal patterns. Corridor 25LD, which takes off from east to west using the South Runway, also shares a similar pattern for the same reason. However, we note that in general the extent of Alert Duration reduction possible over 07RA and 25LD is smaller compared to 07LA. This is possibly due to the fact that 07RA and 25LD is over the South Runway which is closer to the mountains of Lantau Island to the south of HKIA. As a result, they are more susceptible to the influence of smaller-scale (and possibly more intense) wind disturbances directly emanating from the terrain as compared to 07LA over the North Runway which is further from the Lantau Island. These smaller-scale wind disturbances, if reaching the original GLYGA alert thresholds, would be less likely to be removed by GRR as it is designed to filter out smoother wind changes spread over longer distances. Corridor 25RA lands from east to west using the North Runway, while 07RD takes off from west to east using the South Runway. As such their monthly and seasonal patterns are distinct from the previous 3 corridors, and also differ among the two. By inspecting the extent of the blue segments of the histograms we may form an impression of the extent of Alert Duration reduction across the above 5 corridors. A quantitative comparison is shown in Table 1. It gives the total Alert Duration over the whole study period both before and after the application of GRR. The largest reduction (in an absolute sense) occurs over 25LD with a reduction of 1.38% (from 5.24% to 3.86%) while by proportion the largest reduction occurs over 07LA where

the Alert Duration is cut down by more than one-third (from 2.14% to 1.26%). The impact is lowest over 25RA with a change of only 0.06% (from 1.36% to 1.30%). The reason may be related to length-scale of the major wind disturbance leading to windshear encounters. More recent studies [25–27] have reported on the observation and simulation of fine-scale wind features over 25RA down to the hectometric (or a few hundreds of metres) scale which are traceable to PIREP. These fine-scale wind features are associated with the cluster of buildings near the northeastern corner of HKIA, and naturally have spatial scales much smaller than the wind disturbances associated with mountainous terrain. As a result, very few GLYGA-generated windshear alerts could have been removed by GRR procedure.

Table 1. Comparison of Alert Duration before and after application of GRR.

%	07LA	25RA	07RD	07RA	25LD
GLYGA	2.14	1.36	1.63	3.94	5.24
After GRR	1.26	1.30	1.30	3.36	3.86
Reduction	0.88	0.06	0.33	0.57	1.38

Next, we examine the impact of GRR on the hit rate of Lidar-based automatic windshear alerting. The Hit Rate for a corridor is calculated as the percentage of PIREP successfully covered by a windshear alert for that particular corridor. The methodology for calculation of Hit Rate (or percentage of detection, POD) is well-documented in many studies including those focusing on HKIA [4,11,12,27]. We can define the Hit Rate using the following formula:

$$\text{Hit Rate} = \frac{\text{No. of PIREP successfully alerted}}{\text{Total No. of PIREP}} \times 100\% \quad (4)$$

Table 2 compares the Hit Rate before and after application of GRR. As described in Section 2, the number of PIREP may differ significantly across corridors. This results from a combination of meteorological and air traffic management factors, both of which affect the overall runway usage. As such, the Hit Rate, which is a percentage and hence a relative quantity, is a useful metric since it allows the situations across the different runway corridors to be compared in addition to comparing the situation before and after application of GRR. First, we see that the Hit Rate differs across the 5 corridors under consideration, both before and after the application of GRR. This is a natural consequence of the meso-/micro-scale flows arising from the complex natural and built environment around HKIA [28,29], and highlights the challenge of the problem of windshear detection in general. The Hit Rate figures in Table 2 are also in line with values reported in various previous studies dealing with single or combined instrument detection of windshear events at HKIA. It is also important to note that, in real-time operations of HKIA, automatic windshear alerts are provided by an integrated system combining automatic detection output from a suite of observation instruments (including surface anemometers, Terminal Doppler Weather Radar, weather buoys, etc.) in which the Lidars play a part. The Hit Rate values below form a subset of the whole operational system and only reflect the performance of a single data source (i.e., Lidars) which is known to be effective only under clear-air or rain-free conditions. For corridors 07RD and 07RA (respectively, 162 and 132 PIREP), GRR does not lead to any changes in Hit Rate during the study period (respectively, 77 and 90 hits). Over 25RA (393 PIREP), there is a small decrease of the Hit Rate from 60.3% (237 hits) to 59.0% (232 hits). The change is slightly higher over 07LA and 25LD (respectively, 457 and 96 PIREP). For 07LA, the Hit Rate changes from 61.3% (457 hits) to 57.4% (428 hits); for 25LD, from 68.8% (66 hits) to 63.5% (61 hits).

Table 2. Comparison of Hit Rate before and after application of GRR.

%	07LA	25RA	07RD	07RA	25LD
GLYGA	61.3	60.3	47.5	68.2	68.8
After GRR	57.4	59.0	47.5	68.2	63.5
Reduction	3.9	1.3	0.0	0.0	5.2

It may be informative to compare the above figures against related studies pertaining to HKIA. However, there are certain inherent and practical difficulties which would prevent such direct comparison. Firstly, the present study aims at “trimming down” alerts while almost all previous studies focusing on HKIA deal with covering additional missed cases through additional detection principles. As such, one may even say that there is no conceptual equivalent to what is being carried out in this manuscript. Secondly, the present study covers a rather long and recent period, which do not overlap well with previously published reports. For example, in a study covering 2006–2009 [10], a new parameter called the “F-factor”, which is based on the local gradient of the headwind profile, is studied by adding to existing GLYGA alerts (i.e., a logical “OR” operation). While greatly boosting the Hit Rate (by 10% or more), the Alert Duration is also increased—to 5–10% or more where the Hit Rate gain is most conspicuous. In another study [30] covering the spring seasons of 2009 and 2010, the radiometer (a separate remote-sensing instrument installed at HKIA) is used to issue additional windshear alerts on top of GLYGA. The findings, albeit positive, are along a similar vein—boosting the Hit Rate over spring seasons to about 90% would require lengthening the Alert Duration to 15–20%. Given the latest user requirements from the aviation sector, these changes would not have been considered desirable. In addition, in a mathematical or theoretical sense, these cannot be easily “transposed” to a corresponding reduction for comparison either.

We may further compare the fractional (or relative) change in Alert Duration with the fractional change in Hit Rate to demonstrate the impact or effectiveness of GRR. To avoid confusion with the percentage values here reserved for the Hit Rate and Alert Duration, the fractional change will be given in decimal (i.e., a ratio). For illustration, the fractional change in Alert Duration is defined as follows:

$$\text{Fraction change} = \frac{\text{Alert Duration}_{\text{GRR}} - \text{Alert Duration}_{\text{GLYGA}}}{\text{Alert Duration}_{\text{GLYGA}}} \quad (5)$$

where $\text{Alert Duration}_{\text{GRR}}$ represents the Alert Duration after application of GRR and $\text{Alert Duration}_{\text{GLYGA}}$ represents the original Alert Duration (i.e., only using GLYGA). For example, for 07LA, $\text{Alert Duration}_{\text{GRR}}$ is 1.26% and $\text{Alert Duration}_{\text{GLYGA}}$ is 2.14%. Together they give a fractional change of $(1.26\% - 2.14\%) / (2.14\%) = -0.41$. The same applies to other corridors, and to the calculation of the fractional change in Hit Rate. The figures are presented in Table 3. First, the fractional change in Alert Duration echoes the findings in the previous paragraphs, where the reduction is most significant over 07LA (−0.41 which is more than a third) and 25LD (−0.26 which is more than one-quarter). There is a small decrease in the Hit Rate over 07LA, 25RA and 25LD (−0.06, −0.02 and −0.08, respectively) but these all represent less than one-tenth of original number of hits of the respective corridors. We may examine an additional metric which is the ratio between the two fractional changes. A value of one means there is a trade-off between Hit Rate and Alert Duration at an equal proportion. A value exceeding one means a reduction in Alert Duration at the expense of a relatively small drop by proportion in the Hit Rate. Conversely, a value below one means that the reduction in the Alert Duration is only achieved by a proportionately larger drop in Hit Rate. Obviously, larger values of this ratio are more desirable. We can immediately see from Table 3 that the ratio is consistently above 1 for 07LA, 25RA and 25LD. The lowest value for 25RA (2.06) highlights the difficulty in enhancing detection efficiency over that particular corridor, and echoes the earlier discussions about wind disturbances of building-related length-scales. For 07LA (6.47)

and 25LD (3.47), the higher values of the ratio indicate that the application of GRR is by proportion cutting down the Alert Duration in an effective manner, despite the slightly higher drop in Hit Rate as shown in Table 3. For both 07RD and 07RA, the reduction in Alert Duration is essentially achieved with no costs in the Hit Rate (or a ratio tending towards positive infinite), which is close to the limiting, ideal situation.

Table 3. Comparison of fractional change in Alert Duration to fractional change in Hit Rate.

Fractional Change	07LA	25RA	07RD	07RA	25LD
Alert Duration	−0.41	−0.04	−0.21	−0.15	−0.26
Hit Rate	−0.06	−0.02	0.00	0.00	−0.08
Ratio of (Alert Duration/Hit Rate)	6.47	2.06	N/A	N/A	3.47

5. Conclusions

This paper describes the implementation and impact of a new “gentle ramp removal” (GRR) function designed to improve the operational Lidar low-level windshear alerting algorithm at the Hong Kong International Airport (HKIA) known as “GLYGA”. Low-level windshear refers to a sudden change of headwind, with magnitude typically exceeding 15 knots, during the take-off or landing phase of flight at an altitude of 1600 feet (or around 500 m) and is a known aviation safety hazard. At HKIA, Doppler Lidars are employed to perform dedicated “glide-path” scans along the aircraft flight path in order to obtain a best estimate of the headwind component as would be experienced by the landing or departing aircraft. The original GLYGA algorithm then automatically identifies sustained changes in the headwind profile which are converted to an automated alert when predefined thresholds are exceeded. GLYGA is the first operational Lidar-based aviation windshear detection system in the world and has set the benchmark for other airports and many scientific studies since its inception in 2006. Based on feedback and comments from aircraft pilots that certain headwind changes, even with sufficient intensity, might be considered less of a threat if occurring over a longer distance (known as a “gentle ramp”), the GRR function is developed to identify situations where “gentle ramps” are involved such that the corresponding automatic windshear alert could be withheld. The automated procedure for GRR involves identifying those GLYGA windshear ramps where the detected ramp length exceeds 3000 m and withholding the corresponding alert if the root-mean-squared (RMS) fluctuations from the running mean headwind profile fall below 1.2 kt. The GRR thresholds for length-scale and RMS fluctuations are agreed upon with aviation users.

This paper reports on the real-time performance the GRR function after it has been put into operation as part of the Lidar windshear alerting system at HKIA. The study period covers 46 months from March 2016 to December 2019 spanning a total of 2,017,440 min. Five major runway corridors, namely 07LA, 25RA, 07RD, 07RA and 25LD, which account for 1528 out of 1557 (98.1%) of the quality-controlled pilot reports (PIREP) of low-level windshear at HKIA during the study period, are examined. In all 5 corridors the GRR function successfully reduced the respective Alert Duration which is defined as the percentage of time during which a windshear alert, updated every minute by the automatic system, is in force. The reduction is greatest over 07LA (from 2.14% to 1.26%) and 25LD (from 5.24% to 3.86%), and lowest over 25RA (from 1.36% to 1.30%). This behaviour is consistent with literature findings that 25RA, being in close proximity to the building cluster at the northeastern tip of HKIA, is more susceptible to wind disturbances with smaller spatial scales which are not the target for removal by GRR. In terms of the Hit Rate, which is defined as the percentage of PIREP successfully captured by Lidar windshear alerts, the reduction in Alert Duration over 07RD and 07RA are achieved with no change in Hit Rate, which is close to a limiting, ideal situation. For the remaining 3 corridors, the reduction in Alert Duration is achieved in all cases with proportionately smaller decrease in the Hit Rate. Using the ratio of the fractional change in Alert Duration to that of the Hit Rate as a measure of the efficiency of the GRR function, a value of 6.47 and 3.47 are attained, respectively, for 07LA and 25LD. Even for 25RA where the extent of reduction in Alert

Duration is least among the 5 corridors, the ratio still exceeds unity (with value of 2.06). This demonstrates that in all 5 corridors under study GRR is able to effectively reduce the Alert Duration despite their inherent differences due to meteorological conditions and air traffic management configurations. The present study serves as a unique documentation of a real-time enhancement to the world's first Lidar windshear alerting system implemented at a major international airport, and can provide useful reference and example to airports and aviation meteorologists around the world.

Author Contributions: Conceptualization, methodology, writing—review and editing, project administration, P.W.C.; validation, formal analysis, investigation, writing—original draft preparation, K.K.H. All authors have read and agreed to the published version of the manuscript.

Funding: This research received no external funding.

Acknowledgments: Members of the Meteorological Forecast Systems Division of HKO are acknowledged for the initial study and software deployment. The Hong Kong Airline Pilots Association (HKALPA) is gratefully acknowledged for the provision of de-identified aircraft pilot reports to HKO for scientific research. The authors thank the 4 anonymous reviewers who have been helpful in improving the manuscript.

Conflicts of Interest: The authors declare no conflict of interest.

References

1. ICAO. *Meteorological Service for International Air Navigation: Annex 3 to the Convention on International Civil Aviation*, 16th ed.; International Civil Aviation Organization: Montreal, QC, Canada, 2007.
2. ICAO. *Manual on Low-Level Wind Shear and Turbulence*, 1st ed.; International Civil Aviation Organization: Montreal, QC, Canada, 2005.
3. Proctor, F.H.; Hinton, D.A.; Bowles, R.L. A windshear hazard index. In Proceedings of the 9th Conference on Aviation, Range, and Aerospace Meteorology, Orlando, FL, USA, 12–16 September 2000.
4. Shun, C.M.; Chan, P.W. Applications of an Infrared Doppler Lidar in Detection of Wind Shear. *J. Atmos. Oceanic Technol.* **2008**, *25*, 637–655. [[CrossRef](#)]
5. Chan, P.W.; Hon, K.K.; Li, Q.S. A more comprehensive study of terrain-disrupted airflow at the Hong Kong International Airport—Observations and numerical simulations. *Weather* **2019**, *75*, 199–206. [[CrossRef](#)]
6. Hon, K.K. Predicting low-level windshear using 200-m resolution NWP at the Hong Kong International Airport. *J. Appl. Meteor. Climatol.* **2020**, *59*, 193–206. [[CrossRef](#)]
7. Chan, P.W.; Hon, K.K.; Li, Q.S. Documentation of mountain waves observed near Hong Kong International Airport consistent with high-resolution numerical weather prediction model suggestions. *Weather* **2020**. [[CrossRef](#)]
8. Ng, C.W.; Hon, K.K. Fast dual-Doppler LIDAR retrieval of urban boundary layer wind profile. *Weather* **2020**. [[CrossRef](#)]
9. Huang, T.; Li, Y.; Cheng, J.C.H.; Haywood, J.; Hon, K.K.; Lam, D.H.Y.; Lee, O.S.M.; Lolli, S.; O'Connor, E.J.; Lee, H.F.; et al. Assessing Transboundary-local Aerosols Interaction over Complex Terrain Using a Doppler LiDAR Network. *Geophys. Res. Lett.* **2021**, *48*, e2021GL093238. [[CrossRef](#)]
10. Chan, P.W.; Hon, K.K.; Shin, D.K. Combined use of headwind ramps and gradients based on LIDAR data in the alerting of low-level windshear/turbulence. *Meteorol. Z.* **2011**, *20*, 661–670. [[CrossRef](#)]
11. Hon, K.K.; Chan, P.W. Application of LIDAR-derived eddy dissipation rate profiles in low-level wind shear and turbulence alerts at Hong Kong International Airport. *Meteorol. Appl.* **2014**, *21*, 74–85. [[CrossRef](#)]
12. Wu, T.C.; Hon, K.K. Application of spectral decomposition of LIDAR-based headwind profiles in windshear detection at the Hong Kong International Airport. *Meteteorol. Z.* **2018**, *27*, 33–42. [[CrossRef](#)]
13. Zhang, H.; Wu, S.; Wang, Q.; Liu, B.; Yin, B.; Zhai, X. Airport low-level wind shear lidar observation at Beijing Capital International Airport. *Infrared Phys. Technol.* **2019**, *96*, 113–122. [[CrossRef](#)]
14. Zhang, H.; Liu, X.; Wang, Q.; Zhang, J.; He, Z.; Zhang, X.; Li, R.; Zhang, K.; Tang, J.; Wu, S. Low-Level Wind Shear Identification along the Glide Path at BCIA by the Pulsed Coherent Doppler Lidar. *Atmosphere* **2021**, *12*, 50. [[CrossRef](#)]
15. Yoshino, K. Low-level wind shear induced by horizontal roll vortices at Narita International Airport, Japan. *J. Meteor. Soc. Jpn.* **2019**, *97*, 403–421. [[CrossRef](#)]
16. Boilley, A.; Mahfouf, J.-F. Wind shear over the Nice Côte d'Azur airport: Case studies. *Nat. Hazards Earth Syst. Sci.* **2013**, *13*, 2223–2238. [[CrossRef](#)]
17. Nechaj, P.; Gaál, L.; Bartok, J.; Vorobyeva, O.; Gera, M.; Kelemen, M.; Polishchuk, V. Monitoring of Low-Level Wind Shear by Ground-Based 3D Lidar for Increased Flight Safety, Protection of Human Lives and Health. *Int. J. Environ. Res. Public Health* **2019**, *16*, 4584. [[CrossRef](#)] [[PubMed](#)]

18. Weipert, A.; Kauczok, S.; Hannesen, R.; Ernsdorf, T.; Stiller, B. Wind shear detection using radar and lidar at Frankfurt and Munich airports. In Proceedings of the 8th European Conference on Radar in Meteorology and Hydrology (ERAD 2014), Garmisch-Partenkirchen, Germany, 1–5 September 2014.
19. Jones, J.; Haynes, A. A Peak Spotter Program Applied to the Analysis of Increments in Turbulence Velocity. In *Royal Aircraft Establishment Technical Report 84071*; Royal Aircraft Establishment: Bedford, UK, 1984.
20. Woodfield, A.A.; Woods, J.F. Worldwide experience of windshear during 1981–1982. In Proceedings of the AGARD Flight Mechanics Panel Conference on Flight Mechanics and System Design Lessons from Operational Experience (AGARD CP 347), Athens, Greece, 10–13 May 1983; p. 28.
21. Hong Kong Observatory. *Windshear and Turbulence in Hong Kong—Information for Pilots*, 3rd ed.; Hong Kong Observatory: Hong Kong, China, 2010.
22. Chan, P.W.; Shun, C.M.; Wu, K.C. Operational LIDAR-based System for Automatic Windshear Alerting at the Hong Kong International Airport. In Proceedings of the 12th Conference on Aviation, Range, & Aerospace Meteorology, American Meteorological Society, Atlanta, GA, USA, 29 January–2 February 2006.
23. Lee, Y.F.; Chan, P.W. LIDAR-based F-factor for wind shear alerting: Different smoothing algorithms and application to departing flights. *Meteorol. Appl.* **2014**, *21*, 8693. [[CrossRef](#)]
24. Liu, N.K.; Kwong, K.M.; Chan, P.W. Chaotic Oscillatory-based neural network for windshear and turbulence forecast with lidar data. *IEEE Trans. Syst. Man Cybern. Part C (Appl. Rev.)* **2012**, *10*, 1412–1423. [[CrossRef](#)]
25. Hon, K.K.; Chan, P.W.; Chiu, Y.Y.; Tang, W. Application of Short-Range LIDAR in Early Alerting for Low-Level Windshear and Turbulence at Hong Kong International Airport. *Adv. Meteorol.* **2014**, *2014*, 162748. [[CrossRef](#)]
26. Chan, P.W.; Hon, K.K.; Lux, P.; Ngan, K.; Wenig, M. Statistical analysis of building-induced turbulence at an airport. *Atmosfera* **2020**, *34*, 491–502. [[CrossRef](#)]
27. Hon, K.K.; Chan, P.W. Alerting of hectometric turbulence features at the Hong Kong International Airport using a short-range LIDAR. *Meteorol Appl.* **2020**, *27*, e1945. [[CrossRef](#)]
28. Tang, W.; Chan, P.W.; Haller, G. Lagrangian Coherent Structure Analysis of Terminal Winds Detected by Lidar. Part I: Turbulence Structures. *J. Appl. Meteorol. Climatol.* **2011**, *50*, 325–338. [[CrossRef](#)]
29. Tang, W.; Chan, P.W.; Haller, G. Lagrangian Coherent Structure Analysis of Terminal Winds Detected by Lidar. Part II: Structure Evolution and Comparison with Flight Data. *J. Appl. Meteor. Climatol.* **2011**, *50*, 2167–2183. [[CrossRef](#)]
30. Chan, P.W.; Lee, Y.F. Application of a ground-based, multi-channel microwave radiometer to the alerting of low-level windshear at an airport. *Meteorol. Z.* **2011**, *20*, 423–429. [[CrossRef](#)]